Bioorthogonal uncaging of cytotoxic paclitaxel through Pd nanosheet-hydrogel frameworks

Ana M. Pérez-López,[a,¥] *Belén Rubio-Ruiz,*[a,#] *Teresa Valero,*[a] *Rafael Contreras-Montoya,*[d,≠] *Luis Álvarez de Cienfuegos,*[d] *Víctor Sebastián,*[b,c] *Jesús Santamaría*[b,c] *and Asier Unciti-Broceta*[a,*]

[a] Cancer Cancer Research UK Edinburgh Centre, Institute of Genetics and Molecular Medicine, University of Edinburgh, Crewe Road South, Edinburgh EH4 2XR, UK.

[b] Department of Chemical Engineering and Environmental Technology, Institute of Nanosciences of Aragon (INA) and Aragón Materials Science Institute (ICMA), CSIC, University of Zaragoza, 50018 Zaragoza, Spain.

[c] Networking Research Center on Bioengineering Biomaterials and Nanomedicine (CIBER-BBN), 28029 Madrid, Spain.

[d] Departamento de Química Orgánica, Facultad de Ciencias, Universidad de Granada, Campus de Fuentenueva s/n, 18002 Granada, Spain.

Abstract

The promising potential of bioorthogonal catalysis in biomedicine is inspiring incremental efforts to design strategies that regulate drug activity in living systems. To achieve this, it is not only essential to develop customized inactive prodrugs and biocompatible metal catalysts, but also the right physical environment for them to interact and enable drug production under spatial and/or temporal control. Towards this goal, here we report the first inactive precursor of the potent broad-spectrum anticancer drug paclitaxel (a.k.a. Taxol) that is stable in cell culture and labile to Pd catalysts. This new prodrug is effectively uncaged in cancer cell culture by Pd nanosheets captured within agarose and alginate hydrogels, providing a biodegradable catalytic framework to achieve controlled release of one of the most important chemotherapy drugs in medical practice. The compatibility of bioorthogonal catalysis and physical hydrogels opens up new opportunities to administer and modulate the mobility of transition metal catalysts in living environs.

Introduction

Despite the growing impact of molecularly-targeted therapies in cancer, chemotherapy still stands as the main pharmaco-therapeutic choice to treat most kinds of solid malignancies.[1-3] The third-generation cytotoxic drug paclitaxel (**PTX**) is one of the most widely used chemotherapeutics[4,5] and the anticancer drug currently enrolled in more active clinical trials (>1,100)[6]. First isolated from the bark of the Pacific yew tree, the initiation of **PTX**'s phase 2 trials in the 80s raised ecological concerns over the impact on yew populations and sparked the renowned race to complete its total synthesis.[5,7] Nowadays, **PTX** is produced by a semi-synthetic protocol from sustainable sources[7,8] and globally used —alone or in combination— in the treatment of many of the most prevalent types of cancer, including breast, ovarian and lung cancer.[4,5] There are, however, important dose-limiting adverse effects associated to **PTX** therapy (myelosuppression, peripheral neuropathy, cardiac toxicity) that restrains its systemic anticancer efficacy. For that reason, over the last decades much research on **PTX** has been steered to develop efficient drug delivery systems that improve its clinical tolerability[8,9] and low toxicity prodrugs.[10,11] Innovative methods to localize drug activity at the tumor site are still essential to maximize the clinical potential of **PTX**, not least because its ever-growing role in chemotherapy regimens.

The catalytic scope of some of the transition metals most commonly used in chemistry labs has recently expanded from round-bottomed flasks to cell culture plates and animals. Ruthenium,[12-17] palladium,[15-31] gold,[32-34] copper[35,36] or iron-based[37,38] catalysts have demonstrated their compatibility with saline aqueous solutions and their capacity to mediate chemo-specific processes in complex biological systems. The emerging field of bioorthogonal catalysis has enriched the wealth of methods available to label biomolecules,[20,21] release cytotoxic drugs[14,17,24,26,38] or modulate biological functions.[15,16,23,31] In this context, our lab has contributed

to the use of palladium (Pd) as a heterogeneous catalytic system to generate clinically-approved anticancer drugs in living environs.[24,25,39-43] Such an approach aims to achieve increased control over when and where prodrugs are converted into active drugs by exploiting activation strategies that do not rely on metabolic reactions.[44,45] Up to now, non-degradable materials have been used to capture Pd nanoparticles and protect them from the biological milieu, meaning that the devices will stay at the affected tissue even after completing their catalytic function.[41] This situation is certainly useful for cancers that tend to relapse at the same location, but not quite as much for short-lived neoadjuvant therapies or patients with multiple tumor foci. Hence, it would also be desirable to develop implantable systems that securely host Pd nanoparticles to induce local prodrug activation for a limited period of time and, afterwards, degrade and naturally eliminate from the organism.

Here we report the development of a novel **PTX** precursor that exhibits up to 700-fold lower activity than the parent drug and incorporates a Pd-sensitive masking group (Scheme 1). In the presence of Pd catalysts, a rapid depropargylation reaction takes place to trigger the release of **PTX**. In addition, we report the first investigation on the use of physical hydrogels to capture Pd catalysts and their capacity to carry out bioorthogonal uncaging reactions under physiological conditions.

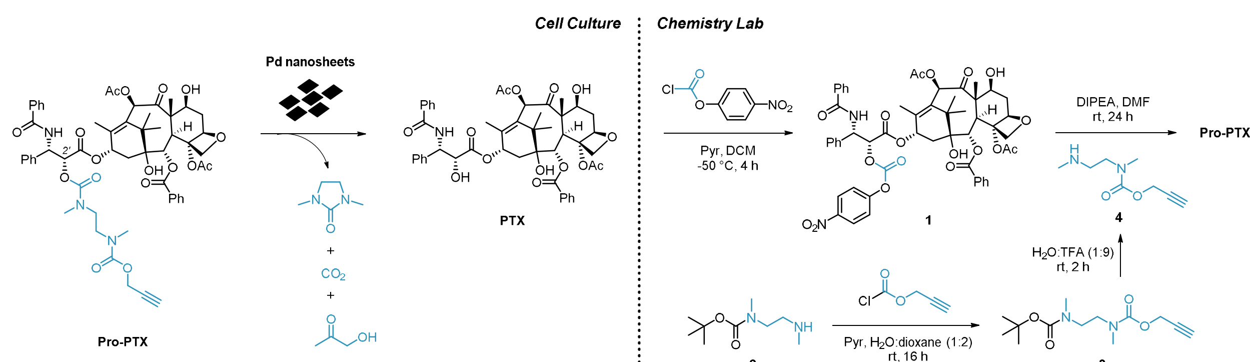

Scheme 1. Proposed Pd-mediated activation strategy in cell culture (left) and synthesis of **Pro-PTX** (right). Cell culture: Pd-mediated *O*-depropargylation of **Pro-PTX** is thermodynamically favored by the generation of CO_2 and designed to trigger an intramolecular cyclization event that releases **PTX** and 1,3-dimethyl-2-imidazolidinone. Dealkylation step in water is expected to afford nontoxic 1-hydroxyacetone.[24] Reaction byproducts could not be confirmed by LCMS. Chemistry lab: Carbamate-protected **Pro-PTX** is semi-synthetically prepared from **PTX** in two steps by successive reactions with *p*-nitrophenyl chloroformate and *N*-(propargyloxycarbonyl)-*N,N'*-dimethylethylenediamine, **4**.

Results and discussion

Design and synthesis of a biochemically stable Pd-sensitive prodrug of PTX. The structure-activity relationships of **PTX** and its analogues have been the subject of intensive research.[46,10] It is well established that one of the essential groups for their bioactivity is the secondary alcohol at the C2' position of the side chain. Masking of this aliphatic OH with various chemical groups (carbonates, esters, carbamates, etc.) has been used to develop **PTX** prodrugs for different purposes.[47,10] In light of previous studies[25] showing that carbamate-based masking groups exhibit significantly higher stability in cell culture than carbonate ones and the need to generate a prodrug that endure the cell metabolism, a bis-carbamate group connected through a *N,N'*-dimethylethylenediamine spacer[48] was used to mask the C2'-OH of **PTX** (Scheme 1). To provide

sensitivity to Pd catalysis, an *O*-propargyl moiety was incorporated at the terminal carbamate that, after cleavage, triggers a self-immolative cascade resulting in the release of **PTX**.

Pro-PTX was prepared following the semi-synthetic route described in Scheme 1 (see the synthetic procedure in the Experimental Section and NMR spectra in the Supp. Inf.). **PTX** was reacted with *p*-nitrophenyl chloroformate in the presence of pyridine to incorporate a reactive carbonate group at its C2'-OH position. Reaction of *N*-Boc-protected ethylenediamine **2** with propargyl chloroformate followed by Boc deprotection under acidic conditions provided compound **4** in high yield (90 %, two steps). Last, coupling of **1** and **4** in the presence of DIPEA generated **Pro-PTX** in moderate yield (36 %).

Cytotoxicity study: PTX vs Pro-PTX. To evaluate the inactivation strategy, viability assays were performed in three cell lines: non-small cell lung carcinoma A549 cells (cell model of human cancer clinically treated with **PTX**),[4,5] human glioblastoma U87 cells (model of aggressive brain cancer)[49] and human brain vascular pericytes (HBVP, non-cancerous cells that are critical components of the blood brain barrier[49] and similar to those found in peripheral nerves). Cells were treated with **PTX** and **Pro-PTX** at a range of concentrations (up to 10 μM) and viability measurements carried out after 5 d of treatment. Results were normalized to the untreated cell control (1% DMSO) and half maximal effective concentration (EC_{50}) values calculated from the generated dose-response curves (see Figure 1). As expected, **PTX** treatment induced a very potent cytotoxic effect against the two cancer cell lines, with EC_{50} values in the range of 2 to 3 nM. In contrast, **Pro-PTX** did not show activity at most concentrations tested in these cell lines, with reduced cell viability only seen at doses ≥1 μM and exhibiting an EC_{50} value of 1.75 μM for A549 and 0.54 μM for U87 cells (Figure 1a,b). This vast drop of anticancer activity (200 to 700-fold lower than **PTX**) highlights the essential role of the C2'-OH of **PTX** for binding its target (lumenal side of microtubules)[4,5] and the stability of the masking group to

enzymatic cleavage and nucleophilic attacks by intracellular biomolecules. As expected, **PTX** and **Pro-PTX** displayed much lower cytotoxicity in low-proliferating HBVP (Figure 1c). Under treatment with **PTX**, cell proliferation was reduced to 75 % at concentrations ≥1 µM, with an EC_{50} value of 0.047 µM. The antiproliferative effect of **Pro-PTX** in HBVP was negligible at most concentrations (EC_{50} = 4.4 µM), which is in agreement with an increased safety profile relative to its parent drug.

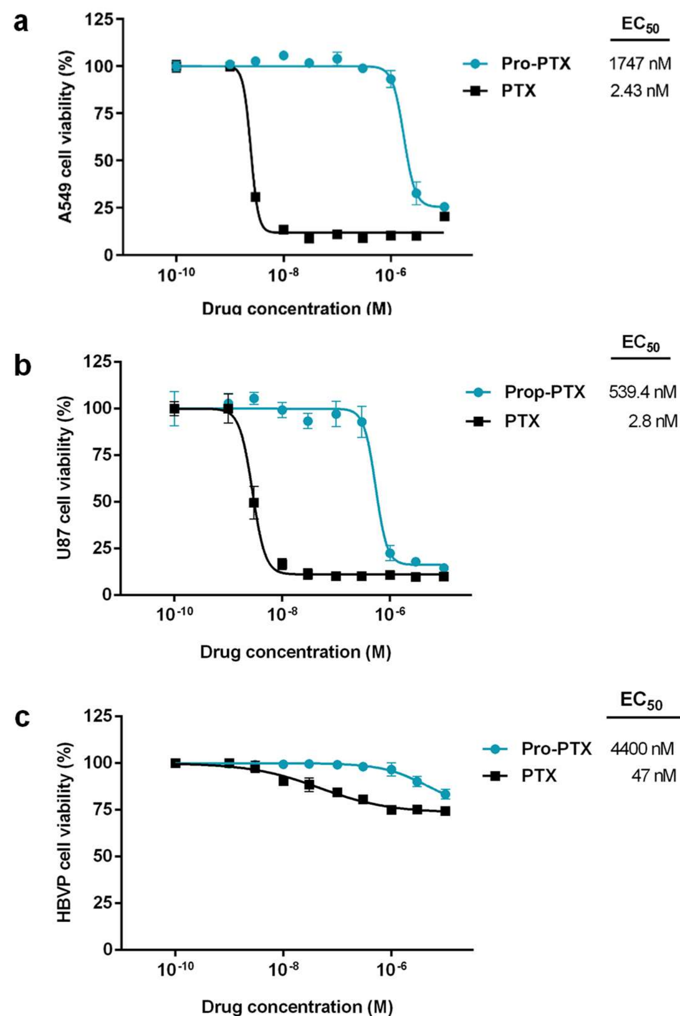

Figure 1. Nine-point semilog dose-response curves and calculated EC_{50} values for (a) A549 cells, (b) U87 cells and (c) HBVP after 5 d treatment with **PTX** and **Pro-PTX** at concentrations ranging from 0.001 to 10 µM. Error bars: ± SEM from n=3.

Prodrug-into-drug conversion studies. Next, the sensitivity of the prodrug to Pd under biologically relevant conditions was tested by incubating **Pro-PTX** at 37 °C in PBS (pH= 7.4, isotonicity) with or without a polymer-supported Pd catalyst, 30 µm **Pd-devices**[41] (which can be easily filtered off to facilitate the analysis of the reaction mixture). Reactions were monitored by MS. While the prodrug remained intact in the absence of Pd (Figure 2a), reaction analysis showed the complete disappearance of the prodrug after 10 h incubation with **Pd-devices** and the formation of major mass peaks corresponding to **PTX** (Figure 2b). The observation of the $[M2+H]^+$ peak in the mass spectrum, which corresponds to the amino derivative **5** (highly-ionizable pre-immolation intermediate), is in agreement with the proposed prodrug activation mechanism.

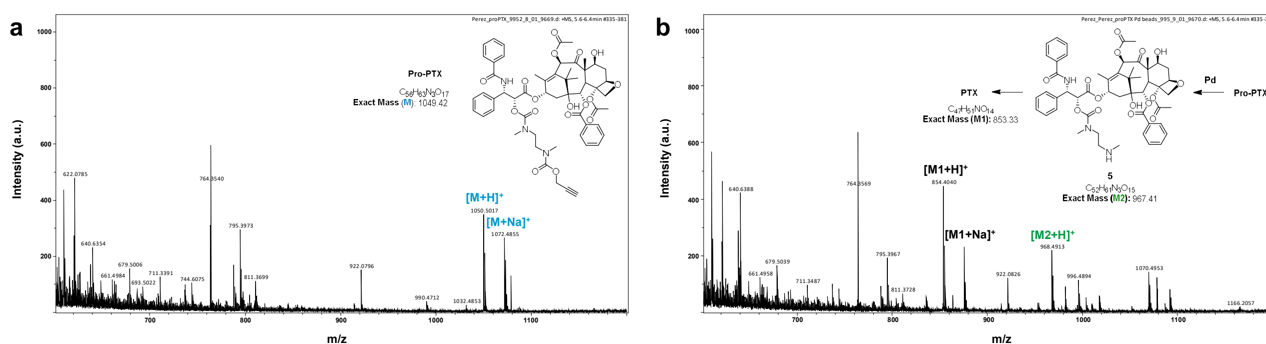

Figure 2. Pd-mediated conversion of **Pro-PTX** into **PTX** under biologically relevant conditions. (a) MS spectrum of **Pro-PTX** (100 µM) after 10 h incubation in PBS at 37 °C. (b) MS spectrum of **Pro-PTX** (100 µM) after 10 h incubation with **Pd-devices** (2 mg/mL) in PBS at 37 °C.

Biodegradable solid supports for Pd catalysts. Bidimensional Pd nanostructures —also called **Pd nanosheets**— have been reported to display good biocompatibility in culture and *in vivo*[50] and, more recently, shown to catalyze bioorthogonal reactions when they are properly protected inside exosomes.[30] Because of their minute size (<2nm in thickness), these ultrathin metallic

structures could be precisely injected at desired anatomical sites (e.g. inside small tumor lesions) and, in time, be eliminated from the organism by the renally and/or the hepatobiliary routes;[51] features that are optimal for short-lived therapeutic applications. However, such small dimensions also make them capable to permeate through most biological barriers, which would defeat the purpose of catalyzing bioorthogonal reactions exclusively at the point of implantation.

Hydrogels are insoluble porous networks with high water content (up to 95%) that have been extensively used as drug reservoirs in controlled release systems.[52] However, the potential use of physical hydrogels as biocompatible scaffolds for bioorthogonal catalysts has never been tested before. Amongst the broad variety of gelling agents available, the FDA-approved natural polysaccharides agarose and alginate are especially attractive for medical and pharmaceutical applications because of their biodegradable and non-thrombogenic nature.[53,54] Driven by the idea of creating implantable catalytic devices capable of uncaging **Pro-PTX** and feature the potential to gradually biodegrade over time, we decided to investigate the use of agarose and alginate-based hydrogels as scaffolds for the immobilization of **Pd nanosheets**.

Pd nanosheets were prepared using a new method (adapted from previous works[55,56,30]) consisting of treating an aqueous solution of Na_2PdCl_4, polyvinyl pyrrolidone and KBr to a CO atmosphere in a high-pressure reactor (6 bar) at 80 °C for 40 min (see full protocol in the Experimental Section). The employ of low toxicity reagents was addressed to increase the biocompatibility of the metallic nanostructures, whereas CO was used as a reductant and capping agent to control the shape and size of the nanoparticles.[55,56] TEM analysis showed the planar and homogeneous shape of the resulting structures (Figure 3a,b), which displayed an average width and thickness of 12 ± 2.2 nm and 1.4 ± 0.1 nm, respectively, making them a priori good candidates to become trapped in polymeric fibrillar networks. Their planar morphology (which

corresponds to less than 9 atomic layers) further agrees with the capacity of the **Pd nanosheets** to absorb in the near infrared range (Figure 3c).[50]

A fluorogenic test was first used to determine the catalyst compatibility with physiological conditions. Reaction was performed by incubation in PBS at 37 °C with the Pd-labile off/on probe *O*-propargyl-resorufin (**Pro-Res**)[30] at a range of concentrations of **Pd nanosheets** (5 to 40 µg/mL in Pd). Changes in fluorescence intensity were measured at 24 h with a spectrophotometer (Ex/Em: 540/590 nm) and conversion rates calculated using a standard curve of resorufin. Analysis revealed dose-dependent fluorescence increases, with conversion rates ranging from 46 to 94% (Fig S3, Supp. Inf.). To determine the fraction of Pd atoms that leaches from the **Pd nanosheets** under the reaction conditions, 20 and 40 µg/mL of **Pd nanosheets** were incubated in PBS at 37 °C during 24 h. The mixture was filtered off using StageTips to eliminate the solid nanostructures and the quantity of soluble Pd in the filtered solution determined by ICP-OES. Analysis detected 8.337 (±3.049) and 16.675 ng/mL (±6.090) of Pd in the samples, respectively, indicating that just a very small fraction of Pd (approx. 0.042 %) leaches from the freestanding **Pd nanosheets** over this period. Next, to test the inherent cytotoxicity of the nanodevices,[57] A549 cells were treated with **Pd nanosheets** for 3 d at the previously tested range of concentrations. Cell viability results showed no signs of toxicity at 5 µg/mL of **Pd nanosheets** and good cell tolerability at 10 µg/mL (Fig S4, Supp. Inf.). Last, a prodrug activation study was performed to corroborate the capacity of the nanodevices to dealkylate **Pro-PTX**. The reaction was performed as described above but using **Pd nanosheets** instead of Pd-functionalized microdevices. The Pd nanodevices were filtered off using StageTips before analyzing the samples by LCMS. Analysis showed the time-dependent disappearance of the prodrug and the formation of the peaks corresponding to **PTX** and the highly-ionizable amino derivative **5** (Fig S5, Supp. Inf.).

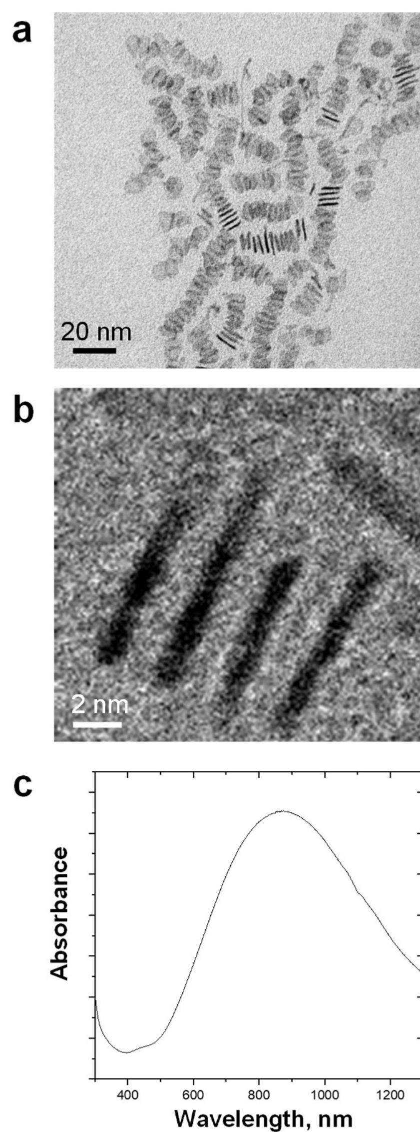

Figure 3. (a,b) TEM images of freestanding **Pd nanosheets** at two magnifications. (c) UV-Vis absorption spectrum of **Pd nanosheets**.

Once the catalytic activity and the biocompatible dose range of the **Pd nanosheets** were confirmed, the use of hydrogels to immobilize these functional nanodevices was investigated. Two biopolymers, agarose and alginate, were tested to take advantage of their different gelling properties and to assess the scope of the capture strategy. Hydrogel formation in the presence of catalysts was first studied by dissolving agarose in warm biological-grade water at a range of

concentrations, followed by mixing with a pre-warmed suspension of **Pd nanosheets**. 60 µL of the mixture were then transferred to tissue culture inserts (0.4 to 8 µm pore) and allowed to cool down to room temperature to generate dark-colored hydrogel disks (**Pd Agarose**) ready to be tested in cell culture (Figure 4a). Optimal catalyst capture was obtained using 5 mg/mL of agarose and 0.4 mg/mL of **Pd nanosheets**.

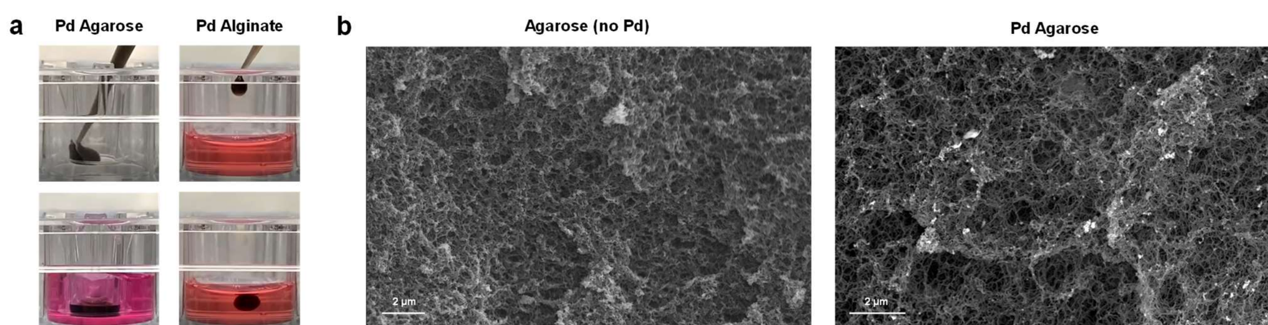

Figure 4. (a) Snapshots of the preparation of **Pd Agarose** and **Pd Alginate** catalytic hydrogels. (b) Representative SEM images of agarose hydrogel (secondary electron detector) and **Pd Agarose** (backscatter electron detector). Bright points observed in the **Pd Agarose** image indicate the presence of metallic Pd.

Next, the uncaging capabilities of the hydrogel-entrapped catalysts from the tissue culture inserts were evaluated by incubation with the off/on probe **Pro-Res** at physiological conditions. Notably, treatment of the probe with **Pd Agarose** (inserts of 1-8 µm pore size) resulted in an increase in fluorescence intensity equivalent to that obtained by freestanding **Pd nanosheets** at the same concentration (Figure 5a). In agreement with the preservation of the catalytic activity, analysis of the hydrogel by SEM shows the apparent capture and homogeneous distribution of the metallic Pd onto the biopolymer fibers (Figure 4b). This indicates that gelification in the presence of a suspension of **Pd nanosheets** favors their trapping and distribution throughout the

fibrillar network with little agglomeration,[58,59] thus increasing the catalytic exposition area while minimizing the escape of the metal. The presence of Pd was further corroborated by Energy Dispersive X-ray (Fig S6, Supp. Inf.).

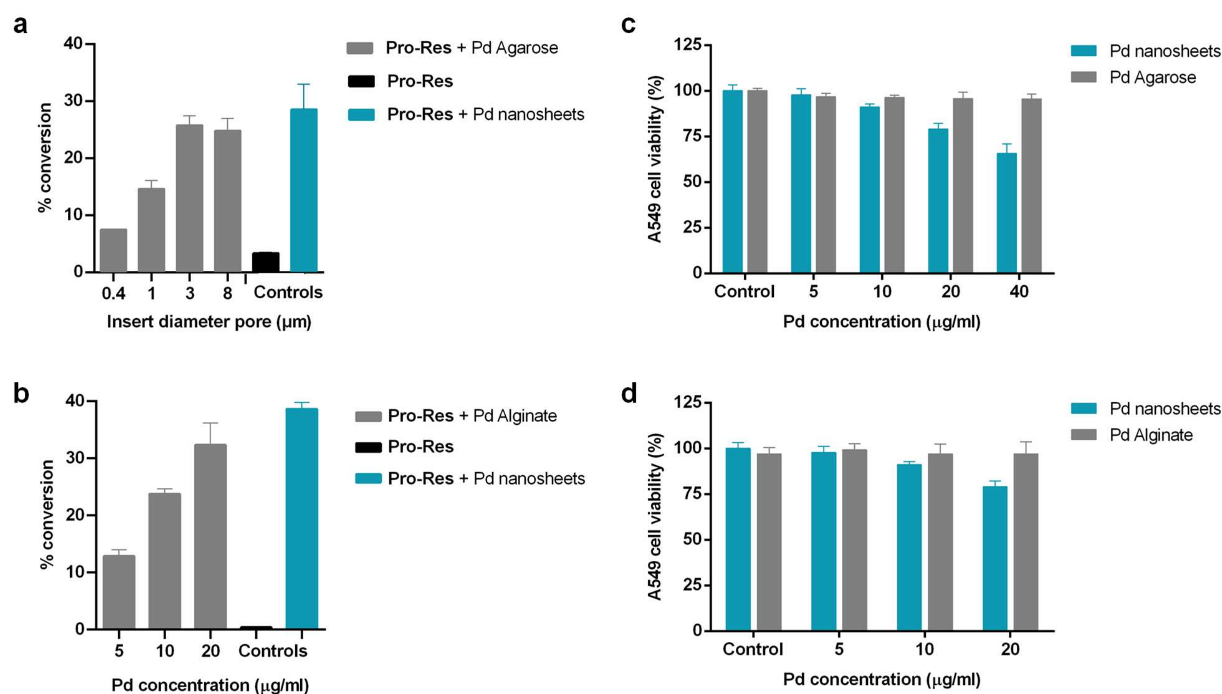

Figure 5. (a,b) Conversion of **Pro-Res** (100 μM) into resorufin by (a) **Pd Agarose** (40 μg/mL of **Pd nanosheets** placed in 0.4-8 μm pore size inserts) or (b) **Pd Alginate** (5 to 20 μg/mL of **Pd nanosheets**) after incubation in DMEM culture media (600 μL or 500 μL, respectively) for 16 h at 37 °C in a tissue culture incubator. **Pro-Res** (100 μM) with or without **Pd nanosheets** were used as negative and positive controls, respectively. Fluorescence signal was measured at $\lambda_{ex/em}$ 540 / 590 nm. Error bars: ± SD from n = 3. (c,d) A549 cell viability study after treatment with (a) **Pd Agarose** and (b) **Pd Alginate** hydrogels at different concentrations. **Pd nanosheets** were included as control. Cell viability was measured at day 3. Error bars: ± SD from n = 3.

Next, because of the capacity of alginate to spontaneously form hydrogels in Ca^{2+} solutions and inspired by previous work from Fortin and coworkers[60] on the "injection & capture" strategy to immobilize radioactive metal nanoparticles in tumors, the entrapment of **Pd nanosheets** was also tested in alginate hydrogels. A suspension of sodium alginate (20 mg/mL) and **Pd nanosheets** (0.3 mg/mL) was first prepared in warm biological-grade water. Then, hydrogels were simply made by dropwise addition of the mixture into PBS or culture media supplemented with 100 mM $CaCl_2$, to generate spherical dark-colored hydrogels (Figure 4a and Movie S1). As before, treatment of the off-on Pd-labile probe **Pro-Res** with **Pd Alginate** spheres demonstrated the functional operativity of the catalytic hydrogel (Figure 5b). Remarkably, cell vitality studies showed that both **Pd Agarose** and **Pd Alginate** hydrogels were better tolerated by A549 cells than freestanding **Pd nanosheets** at equivalent metal concentrations (Figure 5c,d).

Encouraged by the catalytic properties and biocompatibility of the catalyst-loaded hydrogels, the capacity of **Pro-PTX** to enter and be activated by these novel catalytic systems was tested in A549 cells by incubation with **Pro-PTX** in the presence of Pd- or catalyst-free hydrogels. As shown in Figure 6, no reduction of cell proliferation was observed after separately treating A549 cells with either **Pro-PTX** or the catalytic hydrogels. In contrast, the combination of **Pro-PTX** and **Pd Agarose** disk / **Pd Alginate** spheres potently inhibited cancer cell proliferation, resulting in an anticancer activity equivalent to the direct treatment with the parent drug **PTX**. Equivalent results were obtained in the U87 cell line (Fig. S7, Suppl. Inf.). This study demonstrates that, despite its structural complexity, **Pro-PTX** is able to efficiently diffuse across the porous hydrogel network and react with Pd nanosheets to be converted into **PTX**, which then diffuses back through the hydrogel mesh into the culture media.

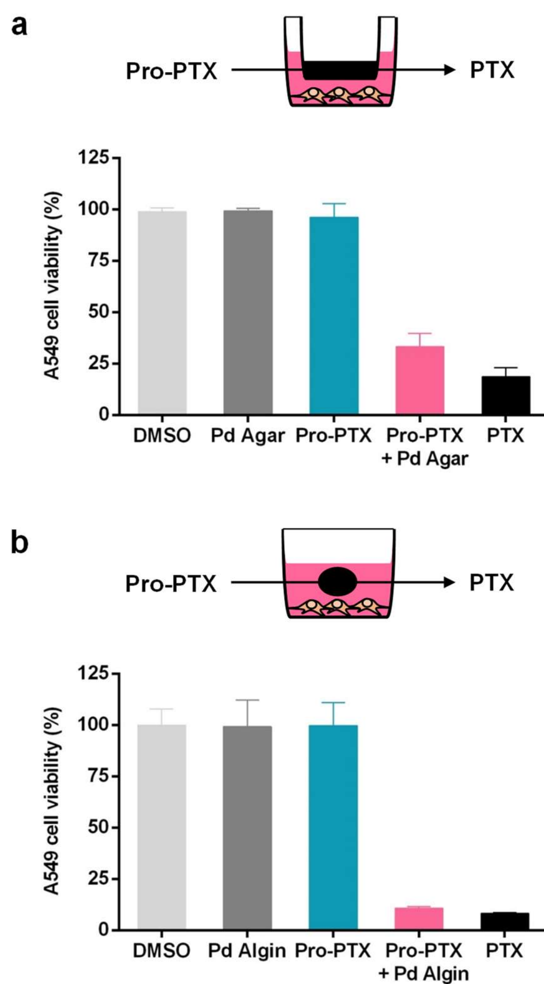

Figure 6. Prodrug activation assays with (a) **Pd Agarose** and (b) **Pd Alginate**. Experiments: 0.1% DMSO (untreated control, light grey); **Pd Agarose** or **Pd Alginate** (–ve control, dark grey); 0.75 µM **Pro-PTX** (–ve control, blue); **Pd Agarose** or **Pd Alginate** + 0.75 µM **Pro-PTX** (activation assay, pink); 0.75 µM **PTX** (+ve control, black). Cell viability was measured at day 3. Error bars: ± SEM, n = 3.

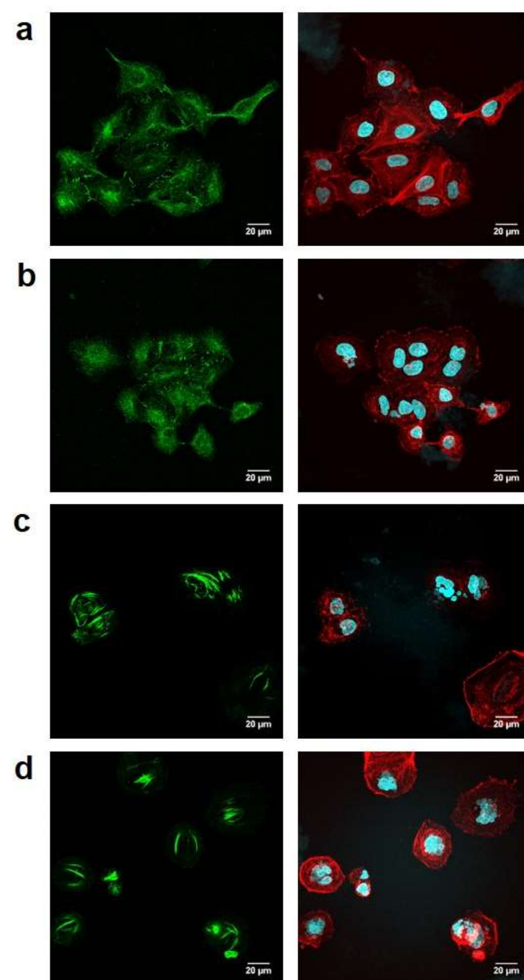

Figure 7. Immunofluorescence study. Experiments: (a) **Pd Alginate**; (b) 0.75 μM **Pro-PTX** + Alginate (no Pd); (c) **Pd Alginate** + 0.75 μM **Pro-PTX** (prodrug activation experiment); (d) 0.75 μM **PTX**. 48 h after treatment, cells were fixed and stained with anti-α-tubulin IgG, TRITC-Phalloidin, and DAPI. Left panels: α-tubulin stain (green). Right panels: nuclei (cyan) and phalloidin (red). Scale bar= 20 μm.

Last, to corroborate that the mechanism of cell death mediated by the **Pro-PTX** / **Pd hydrogel** combination was analogous to that mediated by **PTX**, immunofluorescence studies were performed to image microtubule stabilisation.[4,5] Cells were fixed after 2 d treatment and incubated with an anti-α-tubulin IgG, cell nuclei DAPI stain and TRITC-Phalloidin, and imaged

by confocal microscopy (Olympus FV1000). As observed in Figure 7 (see additional control experiments in Fig S8, Supp. Inf.), whereas controls showed the tubulin signal (green channel) spread throughout the cytoplasm (panels a,b), microtubule accumulation was patently visible after **PTX** treatment (panel d). Importantly, microtubule stabilization was equally evident in cells treated with the **Pro-PTX** / **Pd hydrogel** combination (panel c), thereby proving that the anticancer effect mediated by that combination is a result of the *in situ* formation of **PTX**.

Conclusions

In the exploration of new ways to improve the safety and efficacy of one of the most important anticancer drugs in clinical use, a new prodrug of **PTX** has been developed. This inactive drug precursor features excellent stability in cancer cell culture and high sensitivity to metallic Pd, thus enabling selective drug release in the presence of Pd catalysts. The biscarbamate chemical mask used to block the 2'-OH position of **PTX** provides optimal protection for aliphatic alcohols and metal sensitivity, representing a novel and useful addition to the current toolbox of bioorthogonal uncaging strategies. Moreover, a biocompatible catalytic system based on the immobilization of Pd catalysts in physical hydrogels has been developed for the first time. Entrapment of **Pd nanosheets** in agarose and alginate hydrogels exhibited equivalent catalytic properties than the free catalysts, and displayed the capacity to convert the inactive prodrug **Pro-PTX** into **PTX** in cancer cell culture. By capturing transition metal catalysts within an inherently biodegradable scaffold, this investigation provides a strategy to temporary elicit localized biorthogonal uncaging of chemotherapeutics. As exemplified with alginate, the *in situ* gelling strategy in which a liquid suspension containing catalytic nanodevices solidifies in contact with environs rich in bivalent cations could offer a minimally invasive solution to locally administer and immobilize the catalyst at the disease site. Subsequent studies will focus on progressing these innovations into preclinical animal models.

Experimental section

General Methods. Chemicals and solvents were purchased from Fisher Scientific, Sigma-Aldrich, VWR International Ltd or TCI UK Ltd. **PTX** was purchased from Fluorochem UK. NMR spectra were recorded at ambient temperature on a 500 MHz Bruker Avance III spectrometer. Chemical shifts are reported in parts per million (ppm) relative to the solvent peak. R_f values were determined on Merck TLC Silica gel 60 F254 plates under a 254 nm UV source. Purifications were carried out by flash column chromatography using commercially available silica gel (220-440 mesh, Sigma-Aldrich) or via semipreparative TLC chromatography on Merck TLC Silica gel 60 F254 plates. High Resolution Mass Spectrometry was measured in a Bruker MicrOTOF II. The purity of **PTX** and **Pro-PTX** was >95% for cell studies, as measured by HPLC using an Agilent 1200 system. HPLC method: eluent A: water and formic acid (0.1 %); eluent B: methanol and formic acid (0.1 %); A/B = 95:5 to 5:95 in 4 min, isocratic 2 min (flow = 1 mL / min). Prodrug-into-drug conversion experiments were conducted in a LCMS (Agilent 1200) using a micrOTOF II detector. Method A: eluent A: water and formic acid (0.1 %); eluent B: acetonitrile and formic acid (0.1 %); A/B = 95:5 isocratic 0.5 min, 95:5 to 0:100 in 4.5 min, isocratic 2 min, 0:100 to 95:5 in 0.5 min, and isocratic 2.5 min (flow = 0.2 mL / min). Method B: A/B = 80:20 to 0:100 in 10 min, isocratic 3 min, 0:100 to 80:20 in 5 min (flow = 0.3 mL / min). Stock solutions (100 mM) were prepared in DMSO. SEM images were performed using a FEI Quanta 400 ESEM equipped with an EDX analytical system. A portion of hydrogel was supercriticaly dried and coated with a fine carbon layer. Afterwards, the samples were examined by SEM using secondary and backscatter electron detectors. ICP-OES measurement were carried out in a Varian 715 ICP optical emission spectrometer.

Synthesis of 2’-(4-nitrophenoxycarbonyl)paclitaxel (1). 2’-(4-nitrophenoxycarbonyl)paclitaxel, **1**, was synthesised according to literature procedure.[11]

Synthesis of *N*-(propargyloxycarbonyl)-N,N'-dimethylethylenediamine (4). Tert-butyl methyl[2-(methylamino)ethyl]carbamate, **2** (284 mg, 1.5 mmol) and pyridine (275 µL, 3.4 mmol) were dissolved in a mix of H_2O:1,4-dioxane (3:6, 9 mL). A solution of propargyl chloroformate (221 µL, 2.3 mmol) in 1,4-dioxane (1 mL) was then added dropwise to the mixture at room temperature and the reaction stirred overnight. Subsequently, solvents were removed by rotary evaporation, the crude dissolved in CH_2Cl_2 (20 mL), and the mixture washed with an aqueous solution of 1N HCl (2 x 15 mL) and water (2 x 15 mL). The organic phase was dried over anhydrous $MgSO_4$ and concentrated by rotary evaporation. The crude residue was purified by flash chromatography with 2.5% MeOH in CH_2Cl_2 to give compound **3** as a pale oil. Rf = 0.48 (5% MeOH in CH_2Cl_2). Without further characterization, compound **3** was then dissolved in a 9:1 (v/v) mixture of TFA/water (5 mL) and the mixture stirred at room temperature for 2 h. Solvents were removed by rotary evaporation and the addition of cold diethyl ether (10 mL) afforded pure compound **4** as a yellow solid (90% yield, two steps). Rf = 0.15 (5% MeOH in CH_2Cl_2). **^{1}H NMR** (500 MHz, DMSO-d_6) δ 8.48 (s, 1H), 4.68 (s, 2H), 3.55 (s, 1H), 3.50 (t, J = 6.0 Hz, 2H), 3.08 (t, J = 6.0 Hz, 2H), 2.87 (s, 3H), 2.58 (s, 3H). **^{13}C NMR** (126 MHz, DMSO-d_6) δ 155.8 (C), 79.5 (C), 78.0 (CH), 53.4 (CH_2), 46.5 (CH_2), 45.5 (CH_2), 34.4 (CH_3), 33.2 (CH_3). **HRMS (ESI)** *m/z* $[M + H]^+$ calcd for $C_8H_{15}N_2O_2$, 171.11280; found, 171.11360.

Synthesis of Pro-PTX. Compound **1** (14 mg, 14 µmol) was dissolved in dry DMF (1 mL) under N_2 atmosphere and cooled down to 0°C. Compound **4** (7 mg, 42 µmol) and DIPEA (12 µL, 70 µmol) were dissolved in dry DMF (0.5 mL) and added dropwise to the solution and the mixture allowed to reach room temperature and stirred overnight. The solvent was removed by rotary evaporation and the crude purified by via semipreparative TLC chromatography (2.5% MeOH in CH_2Cl_2) to yield a white solid (36% yield). Rf = 0.40 (5% MeOH in CH_2Cl_2). **^{1}H NMR** (500

MHz, DMSO-d6) δ 9.17 (d, *J* = 8.9 Hz, 1H), 7.98 – 7.94 (m, 2H), 7.87 – 7.81 (m, 2H), 7.73 (t, *J* = 7.5 Hz, 1H), 7.65 (t, *J* = 7.5 Hz, 2H), 7.59 – 7.53 (m, 1H), 7.49 (t, *J* = 7.3 Hz, 2H), 7.47 – 7.43 (m, 4H), 7.19 – 7.17 (m, 1H), 6.29 (s, 1H), 5.87 – 5.81 (m, 1H), 5.66 – 5.54 (m, 1H), 5.41 (d, *J* = 7.2 Hz, 1H), 5.30 – 5.12 (m, 1H), 4.88 (dd, *J* = 14.5, 8.5 Hz, 2H), 4.62 – 4.52 (m, 2H), 4.13 – 4.08 (m, 1H), 4.03 – 3.97 (m, 2H), 3.58 (d, *J* = 7.1 Hz, 1H), 3.46 (d, *J* = 6.6 Hz, 1H), 3.40 (s, 1H), 2.88 (s, 1H), 2.85 (s, 1H), 2.81 (s, 1H), 2.77 (d, *J* = 6.9 Hz, 1H), 2.72 (d, *J* = 0.6 Hz, 2H), 2.35 – 2.20 (m, 4H), 2.10 (d, *J* = 1.5 Hz, 3H), 1.81 – 1.78 (m, 4H), 1.62 (t, *J* = 13.0 Hz, 2H), 1.49 (s, 4H), 1.34 (s, 1H), 1.22 (s, 2H), 1.01 (d, *J* = 7.4 Hz, 6H). **^{13}C NMR** (126 MHz, DMSO-d_6) δ 202.9, 170.1, 169.2, 167.0, 165.7, 155.1, 140.9, 140.4, 137.8, 134.7, 134.0, 131.9, 130.5, 130.1, 129.2, 128.8, 128.6, 128.2, 127.8, 126.8, 116.6, 84.1, 80.7, 79.6, 77.6, 77.2, 76.5, 75.8, 75.2, 75.0, 71.1, 70.9, 66.1, 65.5, 60.2, 57.8, 55.4, 54.5, 52.9, 46.6, 43.4, 37.0, 34.9, 33.7, 32.9, 26.8, 23.0, 21.9, 21.2, 21.1, 20.8, 19.3, 15.6, 14.6, 14.4, 10.2. **HRMS (ESI)** *m/z* $[M + H]^+$ calcd for $C_{56}H_{64}N_3O_{17}$, 1050.42302; found, 1050.42120. Purity as measured by **HPLC** was >99%.

Synthesis of *O*-propargyl-resorufin. Pro-Res was synthesised according to literature procedure.[30]

Cell viability study: PTX vs Pro-PTX. A549 cells (a kind gift from Dr Wilkinson) and U87 cells (a kind gift from Dr Gammoh) were seeded in a 96-well plate format (at 1,500 and 2,000 cells/well, respectively) in DMEM supplemented with 10 % of FBS and L-glutamine (2 mM) and incubated in a tissue culture incubator at 37 °C and 5% CO_2 for 24 h before treatment. HBVP (kind gift from Dr Caporali) were seeded at 10,000 cells (to reach confluency) in pericyte media (ScienCell Research Laboratories, Inc., USA) on gelatin (0.1%) / fibronectin (10µg/ml) pre-coated dishes. Each well was then replaced with fresh media, containing compounds **PTX** and **Pro-PTX** (0.001-10 µM). Untreated cells were incubated with DMSO (0.1 % v/v). After 3 d of incubation, PrestoBlue™ cell viability reagent (10 % v/v) was added to each well and the

plate incubated for 90 min. Fluorescence emission was detected using a PerkinElmer EnVision 2101 multilabel reader (Ex / Em: 540 / 590 nm). All conditions were normalized to the untreated cells (100 %) and curves fitted using GraphPad Prism using a sigmoidal variable slope curve. Experiments were performed in triplicates.

Prodrug-into-drug conversion studies. Pro-PTX (100 μM) was dissolved in PBS (1 mL) with 2 mg of Pd devices (Pd-resins diameter size 30 μm, made as previously reported[41]) and incubated at 37 °C in a Thermomixer at 1,200 rpm during 10 h. Reaction crudes were centrifuged (13,000 rpm, 5 min) to sediment the **Pd-devices** and supernatants were analyzed by LCMS/MS (Agilent 1200) using a micrOTOF II detector. **PTX** (100 μM) was dissolved in PBS (1 mL) for 10 h and analyzed as a positive control.

Preparation of Pd nanosheets. The synthesis of **Pd nanosheets** was based in previous protocols reported,[54,55,30] but with modifications to avoid the use of toxic quaternary ammonium salts. The palladium growth solution was prepared by mixing 11 mg of Na_2PdCl_4, 30 mg of polyvinyl pyrrolidone (MW = 55,000) and 130 mg of KBr in Milli-Q water (400 μL). The resulting homogeneous red solution was mixed with 4 mL of DMF. The Pd nanosheet precursor solution was introduced in a high-pressure stainless-steel Teflon lined reactor. CO gas was introduced in the high-pressure reactor to reduce the Pd precursor and control the anisotropic shape of the Pd nanostructures.[54] The pressure inside the reactor was maintained at 6 bar and the reactor was introduced in a heated water bath (80 ºC for 40 min). The solution was gently stirred with a magnetic flea located at the high-pressure reactor. A dark blue colloid was obtained after the CO treatment. **Pd nanosheets** were collected by centrifugation (10,000 rpm, 10 min) by mixing the dark blue colloid and acetone in a volume ratio of 1 to 3. Finally, **Pd nanosheets** were dispersed in Milli-Q water and kept at 5º C for further use. The Pd concentration was determined by MP-AES (Microwave Plasma-Atomic Emission Spectrometer 4100 Agilent Technologies) and the

optical properties were analysed by UV-VIS spectrophotometry (Jasco V-670). TEM (Tecnai FEI T20) used to study the **Pd nanosheets** morphology by operating at an acceleration voltage of 200 kV with a LaB6 electron source fitted with a SuperTwin® objective lens allowing a point-to-point resolution of 2.4 Å. TEM images showed that the **Pd nanosheets** tend to stack during the drying process of the TEM grid preparation. This effect enabled to observe the ultra-thin sheet like morphology and eased their direct thickness measurement. Leaching of Pd nanosheets after incubation for 24 h in PBS was studied by ICP-OES using a Varian 715 ICP optical emission spectrometer.

Preparation of Pd Agarose. Pd nanosheets were embedded in agarose hydrogels (5 mg/mL) with a Pd concentration of 0.4 mg/mL. Agarose powder (UltraPure™ Agarose, Thermo Fisher Sci.) was weighted in an Eppendorf tube and sterilized by UV radiation. MilliQ water was filtered through a 0.22 µm mesh filter and was added to the agarose powder. The mixture was shacked and warmed at 80 ºC for 5 min to achieve a complete solution. The solution obtained was added on a pre-warmed **Pd nanosheets** suspension and was homogenized by pipetting up and down several times. Immediately after, 60 µL of the suspension were pipetted into tissue culture inserts (Corning Transwell®), placed in a 24 well-plate and allowed to cool at room temperature for 1 h. Afterwards, the 24 well-plate was sterilized under UV radiation for 30 min before characterization and use in cell assays.

Preparation of Pd Alginate. Pd nanosheets were embedded in alginate hydrogels with a Pd nanosheets concentration of 0.3 mg/mL. Sodium alginate powder (Sigma Aldrich, W201502) was dissolved in sterile water and **Pd nanosheets** were added and vortexed until homogenisation. The mixture was sterilised under UV for 15 min. The suspension was added dropwise into standard cell culture medium (DMEM, 10% FBS, 2 mM L-Glutamine) supplemented with 100 mM $CaCl_2$ dihydrate in 24 well-plates to form dark alginate beads. Beads

were washed twice with DMEM and transferred to the experiment wells (3 beads / 500 μL, final concentration of Pd of approx. 20 μg/mL).

Cell toxicity studies: Pd nanosheets vs Pd hydrogels. A549 cells were cultured in DMEM supplemented with 10 % of FBS and L-glutamine (2 mM) and incubated in a tissue culture incubator at 37 °C and 5% CO_2. A549 cells were seeded in a 24-well plate format (at 9,000 cells / well) and incubated for 24 h before treatment. For **Pd nanosheets**, each well was replaced with a suspension of **Pd nanosheets** in fresh culture media at 5, 10, 20 and 40 μg/mL of metal (600 μL final volume). For **Pd Agarose**, each well was replaced with fresh media (540 μL). Agarose hydrogels containing **Pd nanosheets** were prepared following the procedure previously described and placed in cell culture inserts with 1 μm pore size (60 μL, 5-40 μg/mL of metal concentration). For **Pd Alginate**, each well was replaced with fresh media (500 μL). **Pd Alginate** hydrogels were prepared as described above and added at 1-3 beads/well (5-20 μg/mL of metal concentration). After 3 d of incubation, PrestoBlue™ cell viability reagent (10 % v/v) was added to each well and the plate incubated for 180 min. Fluorescence emission was detected using a PerkinElmer EnVision 2101 multilabel reader (Ex / Em: 540 / 590 nm). Experiments were performed in triplicates.

Fluorogenic assays: Pd nanosheets vs Pd hydrogels. Pro-Res (100 μM) was dissolved in DMEM culture media (in 540 μL for **Pd Agarose** hydrogels or in 500 μL for **Pd Alginate** hydrogels) in a 24-well plate format. For **Pd Agarose**, hydrogels containing **Pd nanosheets** at 40 μg/mL (60 μL) were prepared following the procedure above described and placed in cell culture inserts (0.4-8 μm pore size). For **Pd Alginate**, hydrogels containing **Pd nanosheets** at approx. 5-20 μg/mL (1 to 3 beads/well) were prepared following the procedure previously described. **Pd nanosheets** (20 and 40 μg/mL) were used as control. Samples were incubated at 37°C in a tissue culture incubator. **Pd nanosheets** were removed by centrifugation (13,000 rpm, 30 min).

Fluorescence intensity of 100 µL of supernatants transferred to a 96-well plate format was measured in a PerkinElmer EnVision 2101 multilabel reader (Ex / Em: 540 nm / 590 nm). Samples were repeated in triplicate. The percentage of conversion was calculated based on the fluorescence signal of positive control **Resorufin** at 100 µM.

Prodrug activation assays with Pd hydrogels. A549 were seeded in a 24-well plate format (at 9,000 cells / well) and incubated for 24 h before treatment. Each well was replaced with fresh culture media containing **Pro-PTX** or **PTX** (0.75 µM). Untreated cells were incubated with DMSO (0.1 % v/v). **Pd Agarose** and **Alginate** hydrogels (40 µg/mL of metal and 20 µg/mL, respectively) were prepared following the procedure previously described. **Pd Agarose** hydrogels were placed in cell culture inserts with 1 µm pore size and **Pd Alginate** hydrogels added at 3 beads/well. After 3 d of incubation, cell viability was determined as described above. Experiments were performed in triplicates.

Immunofluorescence studies. A549 cells were seeded on 10 mm poly(L-lysine) precoated coverslips in 24 well plates (5,000 cells/well). After 24 h, cells were incubated in the presence or in the absence of alginate gels and/or **Pro-PTX** / **PTX** (0.75 µM) in 500 µL of DMEM in triplicates. After 48 h, cells were fixed with paraformaldehyde (4% v/v) for 10 min and washed 3 times with PBS every 5 min. Cells were permeabilized for 15 min with 0.3% Tween in PBS and washed 3 times with PBS every 5 min. Coverslips were incubated in blocking buffer (1x PBS, 5% Goat serum, 0.3% Triton X-100) for 60 min. Anti-α-tubulin Rabbit mAb (Cell Signaling Technology) was incubated overnight at 4°C in antibody dilution buffer (1x PBS, 1% BSA, 0.3% Triton X-100) at a dilution of 1:25. After washing 3 times with PBS, coverslips were incubated for 30 min in antibody dilution buffer (1x PBS, 1% BSA, 0.3% Triton X-100) with Alexa Fluor 488 Goat anti-Rabbit IgG (H+L) Secondary Antibody (Invitrogen) at a dilution of 1:400. Coverslips were washed three times with PBS and mounted on a slide with a 1:1 mixture of

VECTASHIELD® Hardset™ Antifade Mounting Medium with Phalloidin: VECTASHIELD® Antifade Mounting Medium with DAPI. Cells were imaged using a scanning confocal inverted microscope Olympus FluoView FV1000 (Olympus, Tokyo, Japan) with a 60x oil immersion objective. The images were acquired FV10-ASW program in a sequential mode using software pre-configured settings for Alexa Fluor 488 and TIRTC and analysed with Image-*J* software to obtain maximal projections.

Supporting Information Availability

NMR for **4** and **Pro-PTX**, Figures S1-S8, molecular formula strings, and Movie S1 (preparation of **Pd Alginate**) are available as Supporting Information at…

Conflicts of interest

The authors declare no conflicts of interest.

List of abbreviations

Boc, *tert*-butyloxycarbonyl; DAPI, 4′,6-diamidino-2-phenylindole; DIPEA, *N*,*N*-diisopropylethylamine; DMF, dimethylformamide; DMEM, Dulbecco's modified eagle media; DMSO, dimethylsulphoxide; EC_{50}, half maximal effective concentration; FDA, Food and Drug Administration; ICP-OES, inductively coupled plasma atomic emission spectroscopy; IgG, immunoglobulin G; MP-AES, microwave plasma-atomic emission spectrometer; MS, mass spectrometry; NSCLC, non-small-cell lung carcinoma; PBS, phosphate buffered saline; Pd, palladium; ppm, parts per million; r.t., room temperature; SEM, scanning electron microscopy; SEM, standard error of mean; TEM, transmission electron microscopy; TFA, trifluoroacetic acid; TLC, thin layer chromatography.

Acknowledgements

We thank EPSRC (Healthcare Technology Challenge Award, no. EP/N021134/1) and ERC (Advanced Grant CADENCE, no. ERC-2016-ADG-742684) for funding. BR-R and TV thanks the EC for a MSC Fellowship (H2020-MSCA-IF-2014-658833 and H2020-MSCA-IF-2016-749299, respectively). RCM thanks the support from the Vicerrectorate of Research of University of Granada. RC-M and LAC thanks Junta de Andalucía (Spain) for funding project P12-FQM-790. LAC thanks the Ministerio de Ciencia, Innovación y Universidades for a Salvador de Madariaga visiting professor fellowship (PRX18/00017) and the Agencia Estatal de Investigación (Ministerio de Economia y Competitividad) and the European Regional Development Fund for co-funding project FIS2017-85954-R. VS acknowledges the financial support of Ministerio de Ciencia, Innovación y Universidades, Programa Retos Investigación, Proyecto REF: RTI2018-099019-A-I00.

Author Information

Corresponding Authors

*E-mail: Asier.Unciti-Broceta@igmm.ed.ac.uk. Phone: 0044-(0)-1316518500.

Additional information

[¥] Current address for A.M.P.L.: Technische Universität Berlin, Institut für Biotechnologie, Aufgang 17-1, Level 4, Raum 472, Gustav-Meyer-Allee 25, 13355 Berlin (Germany)

[#] Current address for B.R.R.: Pfizer-University of Granada-Andalusian Regional Government Centre for Genomics and Oncological Research (GENYO) and Department of Medicinal and Organic Chemistry, Faculty of Pharmacy, University of Granada, Granada (Spain)

≠ Current address for R.C.M.: Department of Chemistry, Durham University, South Road, Durham DH1 3LE (U.K).

Notes and references

1. DeVita Jr V. T.; Chu, E. A history of cancer chemotherapy. *Cancer Res.* **2008**, *68*, 8643-8653.

2. Galmarini, D.; Galmarini, C. M.; Galmarini, F. C. Cancer chemotherapy: a critical analysis of its 60 years of history. *Crit. Rev. Oncol. Hematol.* **2012**, *84*, 181-199.

3. Savage, P. Chemotherapy curable malignancies and cancer stem cells: a biological review and hypothesis. *BMC Cancer*, **2016**, *16*, 906.

4. Mekhail, M. T.; Markman. M. Paclitaxel in cancer therapy. *Expert Opin. Pharmacother.* **2002**, *3*, 755-766.

5. Weaver, B. A. How Taxol/paclitaxel kills cancer cells. *Mol. Biol. Cell*, **2014**, *25*, 2677-2681.

6. www.clinicaltrials.org (accessed Mar 30, 2020).

7. Liu, W. C.; Gong T.; Zhu. P. Advances in exploring alternative Taxol sources. *RSC Adv.* **2016**, *6*, 48800-48809.

8. Wang, F.; Porter, M.; Konstantopoulos, A.; Zhang, P.; Cui. H. Preclinical development of drug delivery systems for paclitaxel-based cancer chemotherapy. *J. Control Rel.*, **2017**, *267*, 100-118.

9. Yang, X.-C.; Samanta, B.; Agasti, S. S.; Jeong, Y.; Zhu, Z.-J.; Rana, S.; Miranda, O. R.; Rotello, V. M. Drug delivery using nanoparticle-stabilized nanocapsules. *Angew. Chem. Int. Ed.* **2011**, *50*, 477-481.

10. Meng, Z.; Lv, Q.; Lu, J.; Yao, H.; Lv, X.; Jiang, F.; Lu, A.; Zhang, G. Prodrug strategies for paclitaxel. *Int. J. Mol. Sci.* **2016**, *17*, 796.

11. Dal Corso, A.; Caruso, M.; Belvisi, L.; Arosio, D.; Piarulli, U.; Albanese, C.; Gasparri, F.; Marsiglio, A.; Sola, F.; Troiani, S.; Valsasina, B.; Pignataro, L.; Donati, D.; Gennari, C. Synthesis and biological evaluation of RGD peptidomimetic-paclitaxel conjugates bearing lysosomally cleavable linkers. *Chem. Eur. J.* **2015**, *21*, 6921-6929.

12. Streu, C.; Meggers, E. Ruthenium-induced allylcarbamate cleavage in living cells. *Angew. Chem. Int. Ed.* **2006**, *45*, 5645-5648.

13. Sánchez, M. I.; Penas, C.; Vázquez, M. E.; Mascareñas, J. L. Metal-catalyzed uncaging of DNA-binding agents in living cells. *Chem. Sci.* **2014**, *5*, 1901-1907.

14. Völker, T.; Dempwolff, F.; Graumann, P. L.; Meggers, E. Progress towards bioorthogonal catalysis with organometallic compounds. *Angew. Chem. Int. Ed.* **2014**, *53*, 10536-10540.

15. Tomás-Gamasa, M.; Martínez-Calvo, M.; Couceiro, J. R.; Mascareñas, J. L. Transition metal catalysis in the mitochondria of living cells. *Nat. Commun.* **2016**, *7*, 12538.

16. Okamoto, Y.; Kojima, R.; Schwizer, F.; Bartolami, E.; Heinisch, T.; Matile, S.; Fussenegger, M.; Ward, T. R. A cell-penetrating artificial metalloenzyme regulates a gene switch in a designer mammalian cell. *Nat. Commun.* **2018**, *9*, 1943.

17. Sabatino, V.; Rebelein J. G.; Ward, T. R. “Close-to-Release”: Spontaneous bioorthogonal uncaging resulting from ring-closing metathesis. *J. Am. Chem. Soc.* **2019**, *141*, 17048-17052.

18. Yusop, R. M.; Unciti-Broceta, A.; Johansson, E. M. V.; Sánchez-Martín, R. M.; Bradley, M. Palladium-mediated intracellular chemistry. *Nat. Chem.* **2011**, *3*, 239-243.

19. Unciti-Broceta, A.; Johansson, E. M. V.; Yusop, R. M.; Sánchez-Martín, R. M.; Bradley, M. Synthesis of polystyrene microspheres and functionalization with Pd(0) nanoparticles to perform bioorthogonal organometallic chemistry in living cells. *Nat. Protocols* **2012**, *7*, 1207-1218.

20. Li, N.; Lim, R. K.; Edwardraja, S.; Lin, Q. Copper-free sonogashira cross-coupling for functionalization of alkyne-encoded proteins in aqueous medium and in bacterial cells *J. Am. Chem. Soc.* **2011**, *133*, 15316-15319.

21. Spicer, C. D.; Triemer, T.; Davis, B. G. Palladium-mediated cell-surface labeling. *J. Am. Chem. Soc.* **2012**, *134*, 800-803.

22. Tonga, G.Y.; Jeong, Y.; Duncan, B.; Mizuhara, T.; Mout, R.; Das, R.; Kim, S. T.; Yeh, Y. C.; Yan, B.; Hou S.; Rotello, V. M. Supramolecular regulation of bioorthogonal catalysis in cells using nanoparticle-embedded transition metal catalysts. *Nat. Chem.* **2015**, *7*, 597-603.

23. Li, J.; Yu, J.; Zhao, J.; Wang, J.; Zheng, S.; Lin, S.; Chen, L.; Yang, M.; Jia, S.; Zhang, X.; Chen, P. Palladium-triggered deprotection chemistry for protein activation in living cells. *Nat. Chem.* **2014**, *6*, 352-361.

24. Weiss, J. T.; Dawson, J. C.; Macleod, K. G.; Rybski, W.; Fraser, C.; Torres-Sánchez, C.; Patton, E. E.; Bradley, M.; Carragher, N. O.; Unciti-Broceta, A. Extracellular palladium-catalysed dealkylation of 5-fluoro-1-propargyl-uracil as a bioorthogonally activated prodrug approach. *Nat. Commun.* **2014**, *5*, 3277.

25. Weiss, J. T.; Dawson, J. C.; Fraser, C.; Rybski, W.; Torres-Sánchez, C.; Bradley, M.; Patton, E. E.; Carragher, N. O.; Unciti-Broceta, A. Development and bioorthogonal activation of palladium-labile prodrugs of gemcitabine. *J. Med. Chem.* **2014**, *57*, 5395-5404.

26. Miller, M. A.; Askevold, B.; Mikula, H.; Kohler, R. H.; Pirovich, D.; Weissleder, R. Nano-palladium is a cellular catalyst for in vivo chemistry. *Nat. Commun.* **2017**, *8*, 15906.

27. Miller, M. A.; Mikula, H.; Luthria, G.; Li, R.; Kronister, S.; Prytyskach, M.; Kohler, R. H.; Mitchison, T.; Weissleder, R. Modular nanoparticulate prodrug design enables efficient treatment of solid tumors using bioorthogonal activation. *ACS Nano*, **2018**, *12*, 12814-12826.

28. Hoop, M.; Ribeiro, A. S.; Rösch, D.; Weinand, P.; Mendes, N.; Mushtaq, F.; Chen, X.-Z.; Shen, Y.; Pujante, C. F.; Puigmartí-Luis, J.; Paredes, J.; Nelson, B. J.; Pêgo, A. P.; Pané S. Mobile magnetic nanocatalysts for bioorthogonal targeted cancer therapy. *Adv. Funct. Mater.* **2018**, *28*, 1705920.

29. Martínez-Calvo, M.; Couceiro, J. R.; Destito, P.; Rodríguez, J.; Mosquera, J.; Mascareñas, J. L. Intracellular deprotection reactions mediated by palladium complexes equipped with designed phosphine ligands. *ACS Catal.* **2018**, *8*, 6055-6061.

30. Sancho-Albero, M.; Rubio-Ruiz, B.; Pérez-López, A. M.; Sebastián, V.; Martín-Duque, P.; Arruebo, M.; Santamaría, J.; Unciti-Broceta, A. Cancer-derived exosomes loaded with ultrathin palladium nanosheets for targeted bioorthogonal catalysis. *Nat. Catal.* **2019**, *2*, 864-872.

31. Plunk, M. A.; Alaniz, A.; Olademehin, O. P.; Ellington, T. L.; Shuford, K. L.; Kane, R. R. Design and catalyzed activation of Tak-242 prodrugs for localized inhibition of TLR4-induced inflammation. *ACS Med. Chem. Lett.* **2020**, *11*, 141-146.

32. Tsubokura, K.; Vong, K.K.; Pradipta, A.R.; Ogura, A.; Urano, S.; Tahara, T.; Nozaki, S.; Onoe, H.; Nakao, Y.; Sibgatullina, R.; Kurbangalieva, A.; Watanabe, Y.; Tanaka, K. In vivo gold complex catalysis within live mice. *Angew. Chem. Int. Ed.*, **2017**, *56*, 3579-3584.

33. Pérez-López, A. M.; Rubio-Ruiz, B.; Sebastián, V.; Hamilton, L.; Adam, C.; Bray, T. L.; Irusta, S.; Brennan, P. M.; Lloyd-Jones, G.; Sieger, D.; Santamaría, J.; Unciti-Broceta, A. Gold-triggered uncaging chemistry in living systems. *Angew. Chem. Int. Ed.* **2017**, *56*, 12548-12552.

34. Vidal, C.; Tomás-Gamasa, M.; Destito, P.; López, F.; Mascareñas, J.L. Concurrent and orthogonal gold(I) and ruthenium(II) catalysis inside living cells. *Nat. Commun.*, **2018**, *9*, 1913.

35. Miguel-Ávila, J.; Tomás-Gamasa, M.; Olmos, A.; Pérez, P. J.; Mascareñas, J. L. Discrete Cu(I) complexes for azide–alkyne annulations of small molecules inside mammalian cells. *Chem. Sci.* **2018**, *9*, 1947-1952.

36. Liu, Y.; Pujals, S.; Stals, P. J. M.; Paulöhrl, T.; Presolski, S. I.; Meijer, E. W.; Albertazzi, L.; Palmans, A. R. A. Catalytically active single-chain polymeric nanoparticles: exploring their functions in complex biological media. *J. Am. Chem. Soc.* **2018**, *140*, 3423–3433.

37. Sasmal, P. K.; Carregal-Romero, S.; Han, A. A.; Streu, C. N.; Lin, Z.; Namikawa, K.; Elliott, S. L.; Köster, R. W.; Parak, W. J.; Meggers, E. Catalytic azide reduction in biological environments. *Chembiochem*, **2012**, *13*, 1116-1120.

38. Cao-Milán, R.; Gopalakrishnan, S.; He, L. D.; Huang, R.; Wang, Li-S.; Castellanos, L.; Luther, D. C.; Landis, R. F.; Makabenta, J. M. V.; Li, C.-H.; Zhang, X.; Scaletti, F.; Vachet, R. W.; Rotello, V. M. Thermally gated bio-orthogonal nanozymes with supramolecularly confined porphyrin catalysts for antimicrobial uses. *Chem*, **2020**, *6*, 1113-1124.

39. Weiss, J. T.; Carragher, N. O.; Unciti-Broceta, A. Palladium-mediated dealkylation of n-propargyl-floxuridine as a bioorthogonal oxygen-independent prodrug strategy. *Sci. Rep.* **2015**, *5*, 9329.

40. Rubio-Ruiz, B.; Weiss, J. T.; Unciti-Broceta, A. Efficient palladium-triggered release of vorinostat from a bioorthogonal precursor. *J. Med. Chem.* **2016**, *59*, 9974-9980.

41. Bray, T.L.; Salji, M.; Brombin, A.; Pérez-López, A.M.; Rubio-Ruiz, B.; Galbraith, L. C.A., Patton, E. E., Leung, H. Y.; Unciti-Broceta, A. Bright insights into palladium-triggered local chemotherapy. *Chem. Sci.* **2018**, *9*, 7354-7361.

42. Adam, C.; Pérez-López, A.M.; Hamilton, L.; Rubio-Ruiz, B.; Bray T. L.; Sieger, D.; Brennan, P. M.; Unciti-Broceta A. Bioorthogonal uncaging of the active metabolite of irinotecan by palladium-functionalized microdevices. *Chem. Eur. J.* **2018**, *24*, 16783-16790.

43. Alonso-de Castro, S.; Terenzi, A.; Gurruchaga-Pereda, J.; Salassa, L. Catalysis concepts in medicinal inorganic chemistry. *Chem. Eur. J.* **2019**, *25*, 6651-6660.

44. Weiss, J. T.; Fraser, C.; Rubio-Ruiz, B.; Myers, S. H.; Crispin, R.; Dawson, J. C.; Brunton, V. G.; Patton, E. E.; Carragher, N. O.; Unciti-Broceta, A. *N*-alkynyl derivatives of 5-fluorouracil: susceptibility to palladium-mediated dealkylation and toxigenicity in cancer cell culture. *Front. Chem.* **2015**, *2*, 56.

45. Unciti-Broceta, A. Bioorthogonal catalysis: Rise of the nanobots. *Nat. Chem.* **2015**, *7*, 538-539.

46. Fang, W. S.; Liang, X. T. Recent progress in structure activity relationship and mechanistic studies of taxol analogues. *Mini Rev. Med. Chem.* **2005**, *5*, 1-12.

47. Skwarczynski, M.; Hayashi Y.; Kiso, Y. Paclitaxel prodrugs: toward smarter delivery of anticancer agents. *J. Med. Chem.* **2006**, *49*, 7253-7269.

48. Bouvier, E.; Thirot, S.; Schmidt, F.; Monneret, C. A new paclitaxel prodrug for use in ADEPT strategy. *Org. Biomol. Chem.* **2003**, *1*, 3343-3352.

49. Valero, T.; Baillache, D.; Fraser, C.; Myers, S. H.; Unciti-Broceta, A. Pyrazolopyrimide library screening in glioma cells discovers highly potent antiproliferative leads that target the PI3K/mTOR pathway. *Bioorg. Med. Chem.* **2020**, *28*, 115215.

50. Huang, X.; Tang, S.; Mu, X.; Dai, Y.; Chen, G.; Zhou, Z.; Ruan, F.; Yang, Z.; Zheng, N. Freestanding palladium nanosheets with plasmonic and catalytic properties. *Nat. Nanotech.* **2011**, *6*, 28-32.

51. Poon, W.; Zhang, Y.-N.; Ouyang, B.; Kingston, B. R.; Wu, J. L. Y.; Wilhelm, S.; Chan, W. C. W. Elimination pathways of nanoparticles. *ACS Nano* **2019**, *13*, 5785-5798.

52. Li, J.; Mooney, D. J. Designing hydrogels for controlled drug delivery. *Nat. Rev. Mater.* **2016**, *1*, 16071.

53. Alam, M. T.; Parvez, N.; Sharma, P. K. FDA-approved natural polymers for fast dissolving tablets. *J. Pharm.*, **2014**, 952970.

54. Ruvinov. E.; Cohen, S. Alginate biomaterial for the treatment of myocardial infarction: Progress, translational strategies, and clinical outlook: From ocean algae to patient bedside. *Adv. Drug Deliv. Rev.* **2016**, *96*, 54-76.

55. Sebastian, V.; Smith, C.D.; Jensen, K.F. Shape-controlled continuous synthesis of metal nanostructures. *Nanoscale*, **2016**, *8*, 7534-7543.

56. Herrer, L.; Sebastian, V.; Martín, S.; González-Orive, A.; Pérez-Murano, F.; Low, P. J.; Serrano, J. L.; Santamaría, J.; Cea, P. High surface coverage of a self-assembled monolayer by in situ synthesis of palladium nanodeposits. *Nanoscale*, **2017**, *9*, 13281-13290.

57. Rubio-Ruiz, B.; Pérez-López, A. M.; Bray, T. L.; Lee, M.; Serrels, A.; Prieto, M.; Arruebo, M.; Carragher, N. O.; Sebastián, V.; Unciti-Broceta, A. High-precision photothermal ablation using biocompatible palladium nanoparticles and laser scanning microscopy. *ACS Appl. Mater. Interfaces*, **2018**, *10*, 3341-3348.

58. Contreras-Montoya, R.; Bonhome-Espinosa, A. B.; Orte, A.; Miguel, D.; Delgado-López, J. M.; Duran, J. D. G.; Cuerva, J. M.; Lopez-Lopez, M. T.; Álvarez de Cienfuegos, L. Iron

nanoparticles-based supramolecular hydrogels to originate anisotropic hybrid materials with enhanced mechanical strength. *Mater. Chem. Front.*, **2018**, *2*, 686-699.

59. Contreras-Montoya, R.; Escolano, G.; Roy, S.; Lopez-Lopez, M. T.; Delgado-López, J. M.; Cuerva, J. M.; Díaz-Mochón, J. J.; Ashkenasy, N.; Gavira, J. A.; Álvarez de Cienfuegos, L. Catalytic and electron conducting carbon nanotube-reinforced lysozyme crystals. *Adv. Func. Mater.* **2019**, *29*, 1807351.

60. Laprise-Pelletier, M.; Lagueux, J.; Côté, M. F.; LaGrange, T.; Fortin, M. A. Low-dose prostate cancer brachytherapy with radioactive palladium-gold nanoparticles. *Adv. Healthc. Mater.* **2017**, *6*, 1601120.

TOC Graphic.